Progress in Laser Inscription in Semiconductors by Multiphoton-Initiated Nanosecond Infrared Pulse Absorption

Pol Sopeña*[1], Niladri Ganguly[1], Gabriel Spühler[2], Andrei Selivanau[2], and David Grojo[1]

[1]*Aix-Marseille Université, CNRS, LP3 UMR 7341, 163 Av. Luminy, 13009 Marseille, France*
[2]*Glucoloop AG, Albisriederstrasse 203A, 8047 Zurich, Switzerland*
**Corresponding author's e-mail: pol.sopena-martinez@univ-amu.fr*

Recent advances in high-power nanosecond laser sources in the infrared have led to applications in imaging and ranging. Laser processing can also benefit from these as they potentially trigger nonlinear absorption mechanisms expanding the number of processable materials. Particularly in semiconductors, these result in local intensities modest enough to avoid detrimental nonlinear propagation and pre-focal plasma screening typically observed with ultrashort pulses. Nonetheless, they allow initiating local energy deposition by multiphoton absorption and induce permanent modifications. In this work, we evaluate the potential of two nanosecond sources with different wavelengths to induce volume modifications in silicon and other semiconductors. We first review previous experiments performed at 1.55 μm, to later focus on a systematic study at 2.8 μm, and finally compare the results. In both cases, Si bulk modifications are observed. Interestingly, for 2.8 μm compared to 1.55 μm, we report a decrease in the energy threshold for volume modification with depth, reproducible rear surface modification, and the ability to write through Ge layers. With both configurations, we measure a positive refractive index variation of ~0.5%, suitable for writing light-guiding structures. This shows the potential of nanosecond infrared pulses for writing complex 3D structures turned to Si photonics and microelectronics packaging.

DOI: 10.2961/jlmn.2025.02.2005
Keywords: laser processing, semiconductor, germanium, silicon, mid-infrared, near-infrared, nanosecond

1. Introduction

Semiconductor materials like silicon (Si) or gallium arsenide (GaAs) are opaque to visible light, which allows employing laser sources from the ultraviolet to the near infrared (IR) to modify and structure their surface [1]. At the same time, when trying to modify the bulk, moving to the transparency window from the near-IR and beyond is imperative. Capitalizing on the extremely high intensities of ultrashort laser sources, one would expect that by tightly focusing femtosecond (fs) IR pulses below the surface of Si or other semiconductors, permanent modifications should be obtained due to multiphoton absorption processes. Despite this is routinely performed in dielectrics, with demonstrations like 5D optical memories in glass [2] or 3D fabrication of polymeric microstructures [3], the high refractive index and narrow bandgap of semiconductors impede directly employing the same conditions as in dielectrics [4]. Respectively, these result in focusing limitations, strong nonlinear energy delocalization and plasma effects, hindering high enough energy delivery at the focus to cross the modification threshold in most cases.

With the aim of achieving modification in the bulk of Si and opening the possibilities of laser processing for fabricating complex photonics devices, 3D waveguides, or electronics components, several studies have been conducted. On the one hand, by focusing a fs pulse in the middle of a Si sphere, solid immersion focusing conditions at ~3 numerical aperture (NA) have been reached to produce the first permanent modification inside Si with a fs pulse [5]. However, this proof-of-concept was far from practical implementation for flat wafer processing. On the other hand, by temporally tailoring the pulse, permanent modifications inside Si and GaAs were obtained by employing THz repetition rate trains of fs pulses [6] or trains of two picosecond (ps) pulses to inscribe buried self-organized structures [7]. Alternatively, by relying on longer pulse durations in the ps and nanosecond (ns) regime, the reduced intensities lead to less free carrier generation that significantly decreases the strong pre-focal plasma formation and make possible to achieve bulk modification by a local thermal runaway [8, 9], which would be otherwise hardly achievable with shorter pulses.

Motivated by the benefits of ns IR pulses for semiconductor laser processing, in this paper we explore the below-surface processing capabilities of different wavelengths, triggering nonlinear absorption regimes at different multiphoton order. The use of longer wavelength in the mid-IR could in principle further improve the localization of the interaction by relying on three-photon (3P) absorption processes instead of two-photon (2P). Besides, direct writing of germanium (Ge), transparent beyond 2 μm, and other materials can be considered. In this context, we first carry out a review on different works (performed by others and our group) where modifications in Si were achieved by ns 1.55-μm erbium-doped fiber lasers, the typical wavelength employed for Si volume processing. Later, taking advantage of the appearance of more powerful mid-IR ns laser sources today employed for LiDAR, spectroscopy or surgery applications [10], we explore the use of a 2.5-ns 2.8-μm laser source for semiconductor laser processing.

Altogether, the feasibility of ns IR pulses for semiconductor laser processing is proved, expanding this technology to new materials and applications still unattainable with other temporal regimes and most common laser sources.

2. Methodology review

The employed irradiation setup is schematically represented in Fig. 1, where the optical components were adapted for each laser source. The irradiations carried out with 1.55 μm pulses used a laser source (MWTech, PFL-1550) delivering 5-ns pulses at a repetition rate of 1 kHz. In this case the beam was expanded by factor two (F1 and F2, 100 and 200 mm) and then passed through a half-wave plate (λ/2) and polarizer pair (pol.) to control the energy. The laser beam was focused by either a 0.42 NA or 0.45 NA (theoretical ω_0=1.2 μm, z_R=10 μm in Si) objective lens, for the experiments of waveguide inscription in Si or semiconductor welding, respectively. The maximum deliverable energy for the 0.42 NA objective was 2.4 μJ whereas it was 11 μJ for the 0.45 NA one.

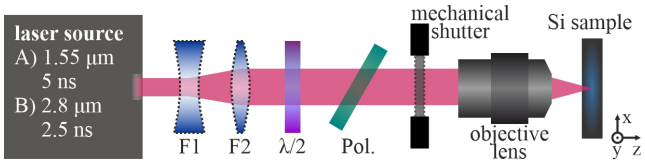

Fig. 1 Schematic representation of the experimental setup comprising the ns laser source, beam expander (F1, F2), λ/2, polarizer, mechanical shutter and focusing objective lens, and semiconductor sample on *xyz* motorized stages.

The same configuration as in Fig. 1 was employed for the mid-IR laser source (Glucoloop AG). It delivered 2.5 ns pulses centered at 2.8 μm at a repetition rate of 800 Hz. The beam expander was removed, and the λ/2 plate and polarizer were adapted for the laser wavelength. The beam was focused on the sample by a 0.56 NA lens (Thorlabs C036TME-D), with theoretical ω_0=1.5 μm and z_R=9 μm in Si. The final delivered energy at the focal point was 6 μJ.

For precise positioning, the sample was mounted on motorized *xyz* stages in all cases. The pulse number was controlled by a mechanical shutter with a minimum aperture time of ~12 ms, leading to the shortest possible irradiations corresponding to trains of 10±1 pulses.

We tested different semiconductors. These comprise Si (intrinsic (100), 1-mm thick, 200–600 Ω·cm, Siltronix), GaAs (intrinsic (100), 600-μm thick, Neyco), indium phosphide (InP; intrinsic (100), 375-μm thick, carrier concentration 0.3–2.0 × 10^{16} cm^{-3}, Biotain Hong Kong Co.), and Ge (n-type (100), 500-μm thick, 5–40 Ω·cm, Neyco). Additionally, we prepared a sample composed of a 2-μm Ge film deposited on a Si wafer by thermal deposition (Edwards Auto 306) for the 2.8 μm laser study.

Surface images of the processed samples were obtained by an optical microscope (Nikon Eclipse LV100ND) and *ex situ* images of the volume modifications were acquired by a transmission microscope coupled to a NIR InGaAs sensor camera (Raptor Photonics Owl 640, 0.6–1.7 μm). Estimations of the refractive index variations of the modifications were performed by an *in-house* phase microscope based on a Mach-Zender interferometer comprising a 1317-nm superluminescent diode (Thorlabs SLD1018S) as light source and the same InGaAs array sensor camera [11].

3. Results and discussion

We carry out different experiments with each laser source. Taking into account the bandgap of Si (1.12 eV), we expect initiating energy deposition by 2P absorption at 1.55 μm whereas it is 3P at 2.8 μm. In this regard, we evaluate the capacity at each multiphoton absorption order to induce permanent modification in Si and other semiconductors.

3.1 Modification of Si at 1.55 μm (2P absorption regime)

The first proof of volume modification of Si in the ns regime was carried out by Verburg et al. [9]. In their study, they employed 3.5-ns pulses centered at 1.55 μm, repetition rate of 100 Hz, and focused inside Si with a 0.7 NA microscope objective (measured ω_0=1.2 μm). By employing 3 μJ pulses they estimated an absorbed energy density at ~1.2×10^4 J/cm^3, which surpasses the required energy for melting (7.1×10^3 J/cm^3). Sending pulses at different energies they obtained modifications by relying on 2P absorption process, finding an approximate threshold at 0.43 μJ (fluence of $F=2E/\pi\omega_0^2$ ~19 J/cm^2). This was later exploited to inscribe several lines at different depths, which served as weak points to precisely dice Si wafers.

In our previous work, we studied the writing of longitudinal light-guiding structures in the bulk of Si by using the 5-ns 1.55-μm source and setup described in section 2 [12]. Changing the main laser parameters (scan speed, 0.1μm/s-1mm/s, and pulse energy, 0.7-2.4 μJ), we identified different structural properties (Fig. 2). As the speed increases, the line width decreased with increasing scan speed (Fig. 2a) and we observed the formation of microcavities and amorphous regions in the phase image in all cases except at intermediate velocities (0.1 mm/s in Fig. 2a). By increasing the pulse energy, the line width (diameter ~6 μm) increased linearly, being able to control its dimensions (Fig. 2b). However, the line uniformity at different speeds seemed to be independent of the pulse energy, finding the most uniform lines at 0.1 mm/s. We evaluated the refractive index change at this speed, finding $\Delta n\sim5.3\times10^{-3}$ ($\Delta n/n\sim0.15\%$). Alternatively, in another work at higher pulse energy densities, we achieved $\Delta n\sim2.6\times10^{-3}$ ($\Delta n/n\sim0.74\%$) [11]. These positive index changes indicated a material transformation consistent with the formation of partially amorphized regions capable of guiding light, as supported by most advanced studies including TEM and Raman [13, 14]. We ultimately demonstrated the ability to guide light through the written channels by coupling light on the waveguide (Fig. 2c). This was done by focusing a 1.55 μm continuous wave (CW) laser diode at the waveguide surface input with a 0.45 NA objective (so that non injected light rapidly spread out after the input), observing how the light scattered along the written structure instead of diffusing away.

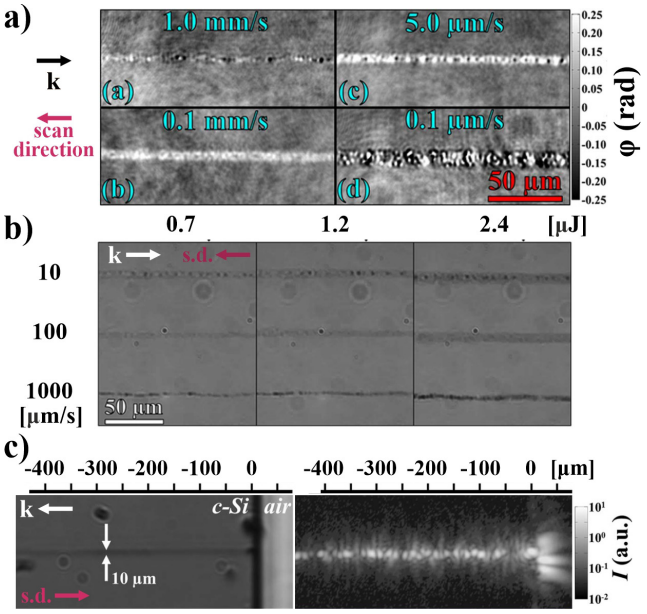

Fig. 2 a) Transverse phase maps of the lines inside Si written at 2 μJ. b) IR transmission images of lines written at different energies and scan speeds. c) Amplitude IR transmission image (left) of a line written at 0.1 mm/s and 2.1 μJ and corresponding scattered light (right) after injecting a 1.55 μm CW laser diode from the left showing the light guiding properties. In all images, the beam was scanned longitudinally; the wave vector k indicates the laser beam direction, and the arrow indicates the scan direction (s.d.). Adapted from [12], with permission.

The capacity of locally modifying below the surface of Si allowed us to investigate the capacity of the same laser source (5-ns 1.55- μm) to laser-weld different semiconductors pieces (including Si and GaAs) [15]. By focusing the beam through the top wafer, at the interface of two pieces in contact, we could identify the conditions to locally melt them and bond them upon resolidification. First, by single-spot irradiations (Fig. 3a), we identified that small imperfections in the Si piece contact can form a Fabry-Perot cavity that prevents modification through the interface. In fact, in the modifications displayed in Fig. 3a-left, we observe a growing backward structure which shape does not change when crossing the interface due to optical contact conditions. However, the appearance of an air gap leads to a cavity resulting in the back reflection of the beam (Fig. 3a-right). By considering optimum optical contact conditions, we later varied the irradiation conditions to determine the most material mixture between wafers without the appearance of detrimental cracks, cavities, or porosities (11 μJ at 2 μm/s). We then raster-scanned the beam to produce a large welded area (Fig. 3b) and, by shear force measurements, we demonstrated a joining strength of 32±10 MPa for the Si-Si configuration. We extended this systematic study to GaAs and tested different configurations alongside Si finding shear joining strengths >10 MPa in all processed cases, one order of magnitude larger than those obtained employing a sacrificial gold layer [16]. This study provided not only the first demonstration of laser welding of similar semiconductors but also dissimilar ones.

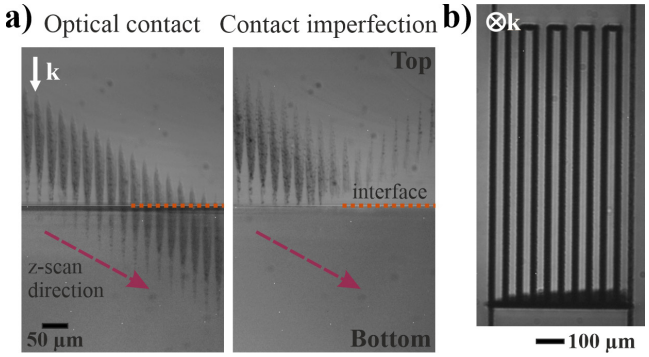

Fig. 3 a) IR transmission lateral view of static modifications at different depths (Δz = 12.5 μm) through a Si-Si interface by sending 1000 pulses at 11 μJ. b) Front IR transmission image of a welded serpentine in the Si-GaAs configuration. Adapted from [15], with permission.

Contrary to previous studies, the 2P absorption process with 5-ns 1.55-μm can also be employed to erase modifications instead of writing [14]. The longer irradiation times of ns pulses compared to ultrashort ones allow 'slowly' heating and cooling during the melting and resolidification process when irradiating a previously induced modification, allowing recrystallization. In this case, we first employed a seeding strategy consisting of a fs pulse that seeded modification by a ps one, writing this way below-surface patterns. This leads to enhanced controllability of the material changes and the possible writing of isolated defects and/or amorphous nanodomains that can be thermally erased. Then, by observing the scattering signal of the irradiated region, we optimized both the axial positioning as well as the pulse energy of the ns pulse, finding complete erasure when sending more than 30 pulses at 0.2 μJ (below the modification threshold of 1.26 μJ with the employed 0.85 NA objective) and a deeper focal shift of 5 μm along the optical axis. We repeated the writing-erasing loop at the same position for 100 cycles, finding that the erasure efficiency starts to decrease from 75 cycles onwards (Fig. 4a). In fact, some local defects remain and tend to accumulate in the irradiated spot, that cannot be further suppressed by nanosecond annealing. Despite this limitation, after 100 reconfigurability cycles the integrated scattering signal of the erased region could be maintained below an arbitrary fixed detection threshold (half of the written structure scattering). While engineering optimizations are needed to target more cycles, this demonstration supports a general vision for enduring non-volatile optical memory applications. Finally, we inscribed different QR codes at the same position below the surface, in which we wrote and erased the different pixels to meet the desired pattern (Fig. 4b). Erasure of ns-written structures had already been demonstrated by oven annealing at 1100 ºC for 2 h [17], but this was the first proof of complete erasing of fs-ps-written spots by ns laser pulses, providing a local technique for reconfigurability applications.

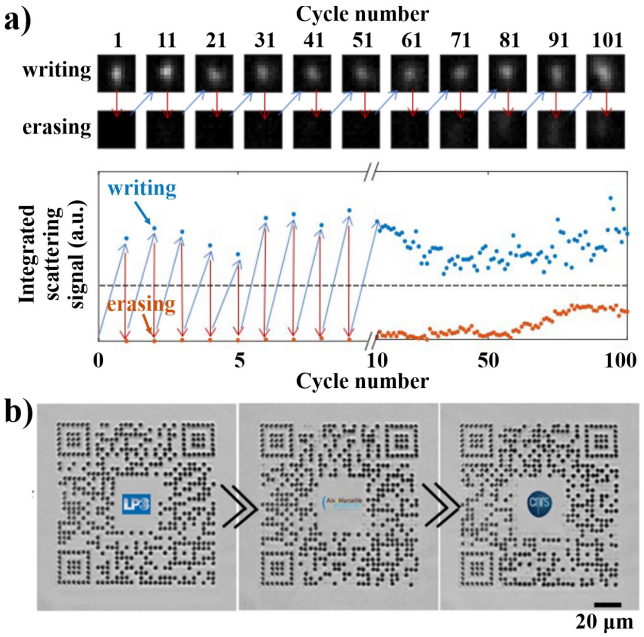

Fig. 4 a) Consecutive writing-erasing cycles employing double pulse seeded writing and 5-ns pulses, respectively. The graph represents the integrated scattering signal from the darkfield microcopy images acquired after each irradiation (examples shown on top). b) Three QR codes subsequently produced at the same location inside a Si wafer (300-µm depth) by applying seeded writing and ns erasure. Adapted from [14], with permission.

Noticeably, Tokel et al. by employing a custom-developed 5-ns fiber laser centered at 1.55 µm were also able to routinely modify the volume of Si [17]. In this case, they employed a 0.75 NA objective and energies of 2-8 µJ to create single-point defects in silicon with spherical resolution of ~1 µm. Then, by seeding from this initial modification and employing a 0.55 NA lens and E~15-20 µJ, they 3D-scanned the beam along the volume to produce complex rod-like structures. With this, they demonstrated several potential applications like optical elements (Fresnel plates, waveguides, optical storing), chemically etched structures (microfluidics, MEMS, surface periodic structures), or oven erasure. Alternatively, by employing the same system and dedicated beam shaping, they were able to produce buried nanostructures with sizes down to 100±20 nm [18]. In this study, the writing of preformed buried structures alongside a Bessel beam resulted in anisotropic feedback providing sub-wavelength control. This allowed them to fabricate polarization-dependent photonic nanostructures or a volume Bragg grating.

3.2 Two- to three-photon absorption at 2.8 µm for modification of semiconductors

After extended works with 1.55 µm ns beams inducing 2P absorption processes in Si and GaAs, we evaluated the capacity of the mid-IR 2.5-ns 2.8-µm laser source to induce in-volume modification in different semiconductors by higher order absorption mechanisms [19].

3-2- 1 Surface writing

Before investigating the ability to modify the volume, we assessed the surface material response. Employing the configuration described in Section 2, we focused on the surface and produced modifications at different energies on different semiconductors including Si, GaAs, InP and Ge.

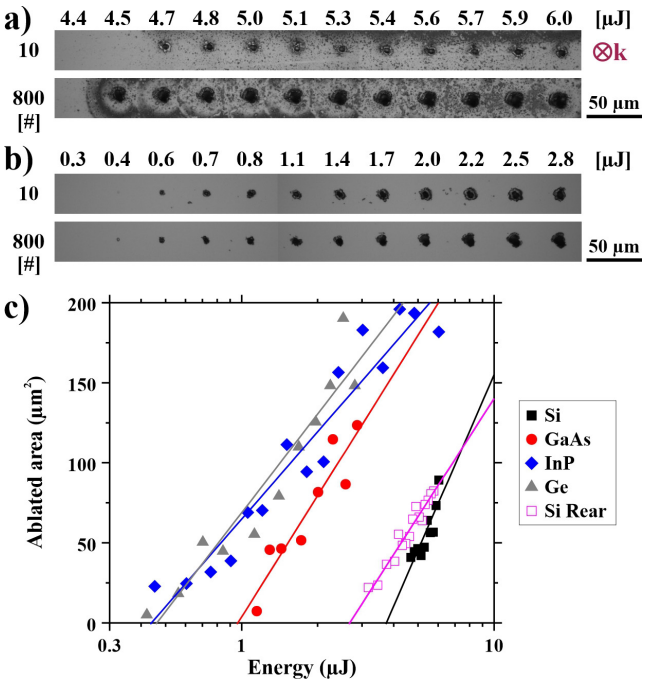

Fig. 5 Optical microscopy images of ablated spots on the surface of a) Si and b) Ge. c) Measured area of the ablation spots performed on Si, GaAs, InP, and Ge at different pulse energies and 10 pulses. Lines correspond to a fit accounting for a thresholding of a Gaussian energy distribution (Table 1). Adapted from [19], with permission.

In Fig. 5a,b we observe images of the obtained ablation spots for both Si and Ge, respectively. The fixed repetition rate of 800 Hz and mechanical shutter of 10 ms resulted in minimum trains of 10 pulses. To determine the incubation effects, we varied the number of pulses from 10 to 800, finding an increasing crater for Si (strong incubation) whereas a rather constant one for Ge (modest incubation). GaAs and InP also showed modest incubation (not shown). Considering the spots performed with 10 pulses, in Fig. 5c we plotted the measured area of the ablated craters versus the pulse energy (log scale) for all samples. Observing the increasing linear trend, we can expect a situation equivalent to Gaussian beam focusing. In this regard, we applied a Liu's fit to all data points [20]. The obtained beam waist and energy threshold are shown in Table 1. The modest incubation observed for GaAs, InP, and Ge, as well as the similar ω_0 indicate a beam radius of around 7 µm (larger than the theoretical one probably due to wavelength mismatch, beam quality, lens filling, and aberrations), which differs from Si due to incubation. From this estimation and E_{th} values we obtain F_{th}~0.5-1 J/cm^2, which are comparable to those routinely found in semiconductors. However, these values should be taken with discretion given the multi-shot limitation of the analysis and are only valid for a dimensional analysis.

Table 1 Significant parameters of the processed semiconductors at 2.8 μm: apparent beam waist (ω_0) and energy threshold (E_{th}), bandgap (BG), multiphoton order (N), material free carrier density (N_e), and multiphoton absorption free carrier density (N_{eN}).

Material	ω_0 [μm]	E_{th} [μJ]	BG [eV]	N	N_e [cm^{-3}]	N_{eN} [cm^{-3}]
Si	10.0	3.74	1.12	3	2×10^{13}	1.7×10^{17}
GaAs	8.3	0.97	1.42	3	--	1.5×10^{17}
InP	7.1	0.44	1.35	3	$0.3\text{-}2\times10^{16}$	1.4×10^{16}
Ge	7.5	0.46	0.67	2	4×10^{13}	5.0×10^{19}

From this, we already identify that despite the modest intensities of ns pulses, we can modify the surface of all semiconductors in a 3P absorption regime for the case of Si, GaAs and InP, whereas it is a 2P process for Ge (Table 1), indicating that volume modification should be possible. However, there could be important collision-assisted mechanisms based on material defects that contribute to absorption. In this regard, we roughly estimated the multiphoton free carrier densities N_{eN} (Table 1) as $N_{EN}=\sigma_N I^N t_p$, where $\sigma_N=\alpha_N/NE_\gamma$ is the multiphoton cross section, N the multiphoton order, I the peak intensity, t_p the pulse duration, α_N the multiphoton absorption coefficient, and E_γ the photon energy. All values and corresponding reference can be found in [19]. Comparing the obtained values to the expected initial free carrier concentrations (N_e) of the materials, we observe that for Si and Ge, the free carrier multiphoton excitation is around four orders of magnitude higher. Thus, general nonlinear absorption might be primarily triggered by multiphoton absorption. However, in the case of InP, the carrier density N_e is similar to the multiphoton one N_{eN}, indicating that material defects are at least partially responsible for initial absorption before a high concentration of multiphoton carriers is created by the pulse. For GaAs, we have no purity characteristics specified by the supplier, but we might expect similar values given the same bi-element nature of the group III-V semiconductor. Taking a closer look at the plot in Figure 5c, we can observe a slightly larger dispersion for GaAs and InP, as well as some missing craters, which might be related to a less deterministic absorption and can be attributed to a sensitivity to material defects.

In this regard, despite all these semiconductors are transparent to the employed wavelength of 2.8 μm, in this comparison, material defects might lead to residual linear absorption. Accounting for the intrinsic nature of the investigated semiconductors, we can expect an electron-hole recombination time larger than the pulse duration (t_p=2.5 ns). Therefore, when we solve the rate equation, we obtain the number of free-electron resulting from linear absorption given by $N_E=\alpha I t_p/E_\gamma$, where α is the linear absorption coefficient. Despite α might be negligible at 2.8 μm, linear absorption is still present from defects, expecting values α in any case under 0.01 cm^{-1} (even if not measurable). By considering this upper value, at the modification threshold intensities, we obtain $N_E \lesssim 10^{16}$ cm^{-3} for the irradiation conditions, showing a process potentially as important as multiphoton ionization as initiator for non-linear energy deposition (including impact and avalanche processes). However, at higher energies (significantly above threshold), since $N_{EN} \propto I^N$, multiphoton absorption is expected to produce more carriers and to progressively become the dominating initiating mechanism.

3-2- 2 In-volume modification

The previous study, showing the ability to induce multiphoton absorption for surface modification, paved the way to irradiate below the surface. In Fig. 5 we focused the 2.8 μm beam 500 μm below the surface of Si and changed the pulse energy and number of pulses. These modifications show the ability to cross the bulk modification threshold in Si relying on 3P absorption with 2.8-μm ns pulses. We found an $E_{th\ vol.} \leq 4.4$ μJ, similar to $E_{th\ surf.}$ (Fig. 2), and larger than the expected value if we account for surface reflection losses (R~30%), which indicates some beam distortions due to nonlinearities or aberration.

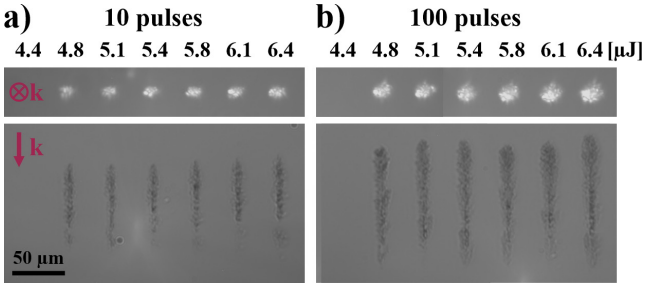

Fig. 6 IR transmission images of volume modifications produced at 500 μm below the surface of Si with a) 10 and b) 100 pulses. Adapted from [19], with permission.

Once we modified at a fixed depth, we performed a continuous scan at different depths through the whole wafer thickness while also changing the pulse energy and employing 800 pulses. The obtained minimum energy for modification (normalized to the surface threshold in Fig. 5) as function of depth for Si is plotted in Fig. 7. We observe the ability to process at different planes and even at the rear-surface, which has been challenging in some previous experiments with different laser conditions [21]. The required energy for volume modification slightly decreases through the wafer and it is even lower on the back surface (~3.8 μJ). This is surprising and opposite to what was observed with 2-μm 7-ns pulses [22], indicating again possible beam aberrations and nonlinear propagation distortions. However, despite our efforts to image the beam profile with an InSb camera, this could not be verified. Additionally, we applied a Liu's fit to the rear surface modification of Si (Fig. 5c), finding a different slope (ω_0 ~ 8.2 μm) compared to the front surface, potentially also indicating the presence of aberrations and nonlinear propagation effects.

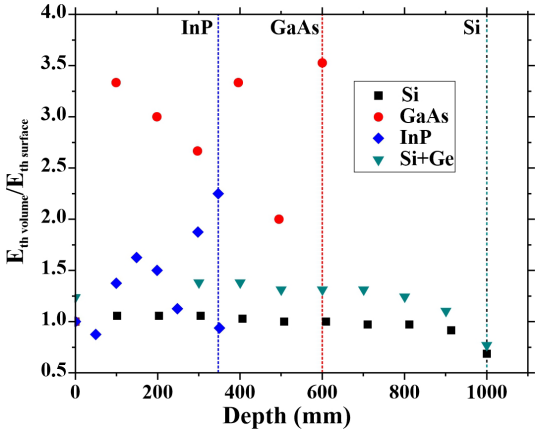

Fig. 7 Volume modification threshold within Si, GaAs, InP, and Si with a 2-µm thick Ge film (Si+Ge). The energy is normalized to E_{th} surface. Dotted vertical lines represent the rear surface of the processed wafers. In all cases the rear surface was modified. Adapted from [19], with permission.

We repeated the same experiment for the other semiconductors, GaAs, InP and Ge, and the results are plotted in Fig. 7. We observe the ability to modify the volume of GaAs and InP at different planes through 3P absorption, with energies 1.5-3 times higher than the surface (accounted by surface losses) but not a clear trend with depth. Despite working in the transparency window of Ge, no bulk modification was detected. We even employed a 0.85 NA aspheric lens (Thorlabs C037TME-D) with no success. This shows that even the low intensities of 2.5-ns pulses, cannot counter the narrow bandgap, high 2P absorption coefficient and negative nonlinear refractive index of Ge that prevent sufficient energy delivery for modification at the focus. By moving to longer wavelengths that would trigger 3P absorption in Ge (~4 µm) and employing better focusing optics, more localized absorption could be expected for a solution to this problem.

Nonetheless, we performed the same study by focusing in Si through a 2-µm thick film deposited on Ge, and we achieved modification in the bulk of Si (Fig. 7), which could not be attained with the 1.55 µm wavelength and highlighting an immediate benefit of mid-IR laser sources.

In view of the random response of volume modification in GaAs and InP (Fig. 7), we performed a repeatability study around the modification threshold. We focused 200 µm below the surface and produced multiple spots at different energies. The modification probability is plotted in Fig. 8. We observe a deterministic trend for Si, whereas GaAs and InP exhibit a wider threshold uncertainty. For Si, the defect density (N_e) is much lower than the multiphoton free carrier ionization (N_{eN}), whereas for InP these are similar (Table 1). Thus, one can expect that absorption in Si is mostly triggered by multiphoton absorption (proved the deterministic threshold transition). On the contrary, the high density of defects in InP can also lead to absorption at energies below E_{th}, and it is only at $E>1.3E_{th}$ that 3P absorption is dominant and the response in InP becomes deterministic. The same reasoning can be translated to GaAs due to the same III-V semiconductor nature. Therefore, there is a competition between defect and multiphoton absorption mechanisms in InP and GaAs that leads to this random response around E_{th}, as observed in other studies [6,23].

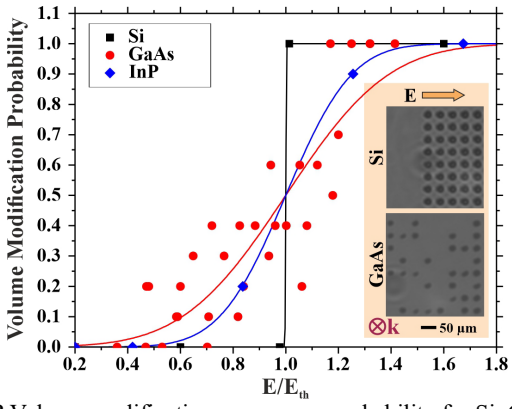

Fig. 8 Volume modification occurrence probability for Si, GaAs, and InP around E_{th}. Insets of performed modifications at increasing energies at 200 µm depth. Fits correspond to the error function. Adapted from [19], with permission.

For a demonstration of the ability of 2.8 µm to address applications, we inscribed the logo of the LP3 laboratory on the surface and different planes (below 300 and 600 µm) inside Si (Fig. 9a). Finally, employing the phase microscope, we measured the refractive index change (Fig. 9b), finding a variation of $\Delta n \sim 1.6\times10^{-2}$ ($\Delta n/n \sim 0.45\%$), which supports, as for experiments at 1.55 µm, an imperfect recrystallization and an apparent partial amorphization [13]. This could be employed to fabricate light-guiding or diffractive structures, as well as other applications like permanent memories, stealth dicing or laser welding.

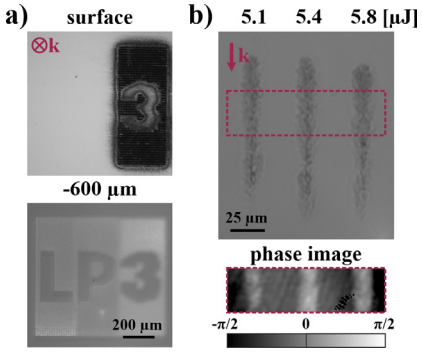

Fig. 9 a) Logo of LP3 laboratory written by individual laser irradiations spots on the surface and volume of Si with 400 pulses at 6 µJ. c) IR-transmission image and corresponding phase image of modifications produced at 500 µm below the surface of Si. Adapted from [19], with permission.

3.3 Benefit of longer wavelength

Direct comparison between experiments conducted with the 1.55 µm and 2.8 µm sources are not evident. Despite both sources showing very similar pulse durations (5 and 2.5 ns, respectively), which should lead to absorption mechanisms discrepancies depending on the multiphoton absorption order, the focusing conditions make the comparison delicate. In order to consider the beam characteristics and provide a common ground for comparison we can evaluate the pulse fluence. Considering Verburg et al. work (Section 3.1) [9], we estimated a fluence modification threshold of ~19 J/cm^2 in the 2P absorption regime. In our case in the 3P absorption window, we obtained F_{th}~6 J/cm^2

(considering E_{th}=4.8 μJ, ω_0=7μm), finding a reduction of the necessary energy for modification at higher multiphoton order (Table 2). In order to induce modification with 3P, one would need in principle more energy than with 2P, due to the higher number of required photons. However, this is not what is observed indicating results that are not governed by a response to a pure multiphoton absorption interaction but there are other important contributions in the energy deposition process.

Similarly, in a previous study of ours where we employed the 1.55 μm ns source described in Section 2 to modify the volume of GaAs, we found that with the 0.45 NA lens the minimum energy for modification was ~0.15 μJ [23]. This approximates to F_{th}~7 J/cm^2 for 2P absorption (Table 2). In the case of 3P at 2.8 μm, we obtained F_{th}~1 J/cm^2 (considering E_{th}=1 μJ, ω_0=7μm). Again, the modification threshold for higher order volume modification in GaAs appears to be lower.

Table 2 Estimated fluence volume modification threshold (F_{th}) and peak intensity (I) for Si and GaAs and the different multiphoton absorption orders (N) and pulse duration (Δt).

Material	Si		GaAs	
N	2	3	2	3
Δt [ns]	3.5	2.5	5.0	2.5
F_{th} [J/cm^2]	19	6	7	1
I (x10^9) [W/cm^2]	5.4	2.4	1.4	0.4

The estimated fluence volume modification threshold for Si and GaAs are then systematically found as smaller when triggered by 3-photon absorption instead of 2-photon absorption (Table 2). This supports a benefit of employing higher multiphoton absorption regimes, as has already been pointed out by M. Chambonneau et al. when performing a spectral absorption study in Si [24]. However, these values in both Si and GaAs should be taken with care given the detected beam distortions in Si (Fig. 7). In addition, the different nonlinear multiphoton coefficients, as well as the differently employed focusing optics, make it hard to strictly compare fluence values from the different studies and make sure that there are no other phenomena like beam distortions coming from nonlinear propagation, plasma screening, or more technical considerations as aberrations. Similarly, for GaAs it was shown in [23] that employing different objectives, only a deterministic response was observed for the tightest focusing (0.85 NA). In this regard, only a dimensional analysis comparison is adequate, and more efforts should be put to make strict comparisons with similar optics and beam quality.

From the volume modification thresholds and the pulse duration we estimated the peak intensity (Table 2), with values in the order of ~10^9 W/cm^2 (if the beam were focused in vacuum) for all cases. Despite these are lower than the ionization value necessary for material modification under multiphoton absorption in dielectric materials with femtosecond pulses (~10^{14} W/cm^2, [25]), the narrow bandgap of semiconductors (Table 1) lead to enough multiphoton absorption of nanosecond pulses to likely promote other mechanisms as impact ionization and avalanche, as well as, a bandgap closure as soon as the temperature is locally increased. This is expected to cause a subsequent runaway of the interaction that result in enough local energy deposition to induce permanent modification. In practice, the lower intensity of nanosecond pulses prevents Kerr-based self-focusing and pre-focal nonlinear and plasma effects, so that effective nonlinear absorption and local thermal runaway can occur at the focus of the beam for permanent modifications hardly achievable with ultrashort pulses [4,9].

Additionally, from experimental evidence, we can identify some benefits by working with mid-IR wavelengths. Compared to 1.55 μm, we achieved wafer modification at different planes without the need of spherical compensation. In fact, we observed a reduction of the threshold energy with depth for the 2.8 μm beam and the inscription on the rear surface without the need of complex configurations [21]. At the same time, narrower bandgap semiconductors than Si are transparent to 2.8 μm, opening the door to process Ge, for example. Even if volume modification in Ge was still not achieved in our study, we demonstrated the ability to process the surface by 2P absorption, as well as modifying through Ge without major beam distortions and opening the doors to multi-layer chip processing. Finally, the last comparison is on the refractive index change. Despite with all wavelengths we are still far from total amorphization (Δn/n~7%) or high densification [26], we obtained in all cases variations of around 0.5%, finding slightly higher values of almost 1% for 1.55 μm [11], which leads to a phase-tuning structure capable of guiding light or manipulating wavefronts.

4. Conclusions

Motivated by light detection and ranging applications, the advent of more intense IR ns laser sources has opened the possibility to use them in laser processing applications. By employing two laser sources centered at 1.55-μm and 2.8-μm, respectively, we reviewed and discussed the possibility to process the bulk of Si and other semiconductors like GaAs, InP and Ge. The different wavelengths but similar nanosecond pulse duration allowed us to set conditions to compare the influence of the multiphoton absorption order. The 1.55 μm Er-doped fiber laser relies on two photon absorption for the case of Si and allowed us to inscribe light-guiding structures in Si, weld different pieces of Si and GaAs, and erase modifications in Si for reconfigurability applications. With the 2.8 μm source, we successfully modified the surface, bulk, and rear surface of Si, GaAs, InP by three photon absorption mechanisms. Compared to 1.55 μm, with the mid-IR source we observe an apparent decrease in the volume modification threshold that decreases with the focusing depth and precise rear-surface modification. This indicates beams largely modified during in-volume propagation.

Despite the 2.8-μm wavelength is transparent to Ge (λ>2μm), the two-photon absorption only allows inducing modification on the surface. In this spectral domain, Ge exhibits a very high two photon absorption coefficient and negative nonlinear refractive index that, alongside enhanced aberrations by the high refractive index, result in beam delocalization and propagation distortions impeding bulk inscription. Still, by irradiating the bulk of Si through a 2-μm thick Ge film deposited on it, we were able to mod-

ify below the surface and already put into evidence important advantages of using 2.8 μm instead 1.55 μm. With a special interest in laser processing for semiconductor-based optics and photonics, we estimated a positive refractive index variation of Δn/n~0.5% with internal structuring of Si for both wavelengths. This must allow creating functional 3D waveguides not only in Si but also other semiconductors and opening new perspectives for new emerging technologies for microelectronics packaging applications including semiconductor laser bonding and dicing.

Acknowledgments

This work was conducted using LaMP facilities at LP3. The project received funding from the French National Research Agency (ANR-22-CE92-0057-0, KiSS project) and the European Union's Horizon 2020 research and innovation program under grant agreements No. 101034324 (MSCA-COFUND) and No. 724480 (ERC).

References

[1] A. Blumenstein, P. Simon, and J. Ihlemann, Nanomaterials, 13, (2023) 2240.
[2] H. Wang, Y. Lei, L. Wang, M. Sakakura, Y. Yu, G. Shayeganrad, and P.G. Kazansky,. Laser Photon. Rev., 16, (2022) 2100563.
[3] K. Sugioka, and Y. Cheng, Light Sci. Appl., 3, (2014) e149.
[4] M. Chambonneau, D. Grojo, O. Tokel, F.Ö. Ilday, S. Tzortzakis, and S. Nolte, Laser Photon. Rev., 15, (2021) 2100140.
[5] M. Chanal, V.Y. Fedorov, M. Chambonneau, R. Clady, S. Tzortzakis, and D. Grojo, Nat. Commun., 8, (2017) 773.
[6] A. Wang, P. Sopeña, and D. Grojo, Int. J. Extreme Manuf., 4, (2022) 045001.
[7] M. Mori, Y. Shimotsuma, T. Sei, M. Sakakura, K. Miura, and H. Udono, Phys. Status Solidi A, 212, (2015) 715.
[8] A. Das, A. Wang, O. Uteza, and D. Grojo, Opt. Express, 28, (2020) 26623.
[9] P. C. Verburg, G. R. B. E. Römer, and A. J. Huis in't Veld, Opt. Express, 22, (2014) 21958.
[10] X. Li, X. Huang, X. Hu, X. Guo, and Y. Han, Opt. Laser Technol., 158, (2023) 108898.
[11] Q. Li, M. Chambonneau, M. Chanal, and D. Grojo, Appl. Opt., 55, (2016) 9577.
[12] M. Chambonneau, Q. Li, M. Chanal, N. Sanner, and D. Grojo, Opt. Lett., 41, (2016) 4875.
[13] L. Trinh, X. Wang, X. Zhang, S. Hosseini-Zavareh, A. Mao, X. Yu, S. Lei, and B. Cui, Adv. Eng. Mater., 26, (2023) 2301377.
[14] D. Grojo, A. Wang, A. Das, V. Fedorov, P. Sopeña, and S. Tzortzakis, 15 July 2024, preprint available at Research Square. 10.21203/rs.3.rs-4636519/v1
[15] P. Sopeña, A. Wang, A. Mouskeftaras, and D. Grojo, Laser Photonics Rev., 16, (2022) 2200208.
[16] M. Chambonneau, Q. Li, M. Blothe, S.V. Arumugam, and S. Nolte, Adv. Photonics Res., 4, (2023) 2200300.
[17] O. Tokel, A. Turnalı, G. Makey, P. Elahi, T. Çolakoğlu, E. Ergeçen, Ö. Yavuz, R. Hübner, M.Z. Borra, I. Pavlov, A. Bek, R. Turan, D. K. Kesim, S. Tozburun, S. Ilday, and F. Ö. Ilday. Nat. Photonics, 11, (2017) 639.
[18] R.A. Sabet, A. Ishraq, A. Saltik, M. Bütün, and O. Tokel, Nat. Comm., 15, (2024) 5786.
[19] P. Sopeña, N. Ganguly, G. Spühler, A. Selivanau, and D. Grojo, Opt. Laser Technol., 179, (2024) 111419.
[20] J.M. Liu, Opt. Lett., 7, (1982) 196.
[21] S. Lei, D. Grojo, J. Ma, X. Yu, and H. Wu, Procedia Manuf., 5, (2016) 594.
[22] N. Gehlich, T. Bonhoff, L. Sisken, M. Ramme, C. Gaida, M. Gebhardt, I. Mingareev, L. Shah, and M.C. Richardson, Utilizing the transparency of semiconductors via "backside" machining with a nanosecond 2 μm Tm:fiber laser, in: U. Klotzbach, K. Washio, C.B. Arnold (Eds.), Laser-Based Micro- and Nanoprocessing VIII, 2014: p. 89680W.
[23] A. Das, A. Wang, O. Utéza, and D. Grojo, Opt. Express, 20, (2022) 39101.
[24] M. Chambonneau, M. Blothe, V.Y. Fedorov, I. Kernier, S. Tzortzakis, and S. Nolte, arXiv, preprint, (2025) arXiv:2504.14908.
[25] F. Krausz, and T. Brabec, Rev. Mod. Phys., 72, (2000) 545.
[26] M.J.A. de Dood, A. Polman, T. Zijlstra, and E.W.J.M. van der Drift, J. Appl. Phys., 92, (2002) 649.

(Received: April 1, 2025, Accepted: July 20, 2025)